JMEPEG (2024) 33:1827–1841
https://doi.org/10.1007/s11665-023-08089-9

1059-9495/$19.00

TECHNICAL ARTICLE

Preparation and Tribological Properties of Potassium Borate/Graphene Nano-composite as Lubricant Additive

Xianbin Hou, Xiang Liu, Leyang Dai, Yuhao Yang, Jinhong Du, Yongjian Wang, Hong Wan, and Xiang Rao

Submitted: 5 November 2022 / Revised: 24 January 2023 / Accepted: 5 February 2023 / Published online: 16 March 2023

Abnormal wear of the cylinder liner and piston ring in a marine diesel engine will lead to the failure of the diesel engine and colossal energy loss. Using lubricating oil additive with good anti-friction and anti-wear properties effectively inhibits the abnormal wear of cylinder liner and piston rings in diesel engine. The potassium borate/graphene (PB/GN) nano-composite lubricant additive suitable for a marine diesel engine was prepared in this study. Its tribological properties in 500 N base oil were investigated using a pin-on-disk tribotester under various loads and temperature. The frictional surface was comprehensively analyzed using field emission scanning electron microscopy (FESEM), energy dispersive spectrometer (EDS), x-ray photoelectron spectroscope (XPS) and Raman to explore the lubrication mechanisms of the PB/GN nano-composite additive. The results indicated that the PB/GN nano-composite additive could substantially improve the tribological performances of 500N base oil. This could be attributed to the good thermal conductivity of graphene and the tribofilms composed of C, FeO, Fe_2O_3 and B_2O_3 formed on the worn surface. The synergy of PB and GN enhanced the tribological performances of base oil.

Keywords graphene, lubricant additive, potassium borate, tribological properties

1. Introduction

As is well known, the failures of diesel engines and huge energy loss are mainly attributed to the friction and wear of the diesel engine moving parts, which can cause the capacity loss of diesel engines to 70% (Ref 1-3). The appropriate lubricant additive can effectively relieve the problem by enhancing the lubricating performance of oil and reducing friction and wear (Ref 4, 5). Therefore, developing high-performance lubricant additive under high speed, high temperature and high load conditions is important to reduce wear damage in the diesel engine. Nano-additive exhibiting good thermal stability, high mechanical strength, special structure and outstanding tribological properties have drawn the attention of researchers.

Graphene has attracted the strong interest of researchers in the lubricant additive field because of its special laminated structure, high mechanical strength, excellent thermal conductivity, remarkable super lubricating properties and high load-bearing capacity (Ref 6-9). Rasheed et al. (Ref 10) investigated the tribological performances of multilayer graphene when adding 0.01 wt.% graphene to engine lubricating oil. The results indicated that the friction shear force broke the graphene with a large size and temperature change between the piston ring and cylinder liner. The suspension bond of graphene fragments made graphene firmly adsorbed on the surface of the piston ring and formed a protective film, which can prevent direct contact between the piston ring and cylinder liner under a high pressure of about 0.5 Gpa. The friction coefficient of engine oil with 0.01 wt.% graphene was reduced by 21%, and the thermal conductivity improved by 23% at 80 °C. Paul et al. (Ref 11) prepared dodecylamine functionalized graphene by solution mixing and investigated the tribological performances of graphene in 500 N engine oil. The results indicated that the friction coefficient was reduced by 40% when adding 0.1 wt.% graphene in engine oil. The tribological performance was improved because the friction chemical films of C and Fe_2O_3 formed on the friction surface, reducing friction and wear.

As a lubricant additive, borate has non-toxicity, odorless, anti-corrosion, anti-rust and good eco-friendly performance and thermal oxidation stability, excellent extreme pressure and anti-wear properties (Ref 12). Many studies have shown that borate nanomaterials as lubricant additive can effectively enhance the lubricating properties of the base oil. Wang et al. (Ref 13) prepared borate ester containing a phenylboronic group (BDDP) and comparatively investigated the tribological performance of BDDP, commercial additive Zinc Dialkyl Dithiophosphates (ZDDP) and F10A in PAO 6 base oil, and found

Xianbin Hou, Fujian Provincial Key Laboratory of Naval Architecture and Ocean Engineering, School of Marine Engineering, Jimei University, Xiamen 361021 Fujian, People's Republic of China; and Key Laboratory of Beibu Gulf Offshore Engineering Equipment And Technology, College of Marine Technology, Beibu Gulf University, Qinzhou 535011 Guangxi, People's Republic of China; **Xiang Liu, Leyang Dai, Yuhao Yang,** and **Yongjian Wang**, Fujian Provincial Key Laboratory of Naval Architecture and Ocean Engineering, School of Marine Engineering, Jimei University, Xiamen 361021 Fujian, People's Republic of China; **Jinhong Du**, Equipment Administration Dept, CCCCSDC (Fujian) Communication Construction Engineering Co., Ltd, Xiamen, People's Republic of China; **Hong Wan**, Key Laboratory of Beibu Gulf Offshore Engineering Equipment And Technology, College of Marine Technology, Beibu Gulf University, Qinzhou 535011 Guangxi, People's Republic of China; and **Xiang Rao**, Key Laboratory of Marine Power Engineering & Technology (Ministry of Transport), Wuhan University of Technology, Wuhan 430063, People's Republic of China. Contact e-mails: daileyang@jmu.edu.cn and fredwh@bbgu.edu.cn.

that the base oil with 0.8 wt.% BDDP possessed a better tribological performance than those of ZDDP and F10A. The analyses showed that the excellent tribological properties of BDDP in PAO were attributed to the formation of tribofilms composed of Fe_2B, B and B_2O_3 on the worn surfaces. Li et al. (Ref 14) prepared the potassium borate nano-particles (nPB) with a spray drying process and explored the lubricating properties of nPB and conventional additive ZDDP in PAO base oil. The test showed that the lubricating properties of nPB superior to that of the ZDDP, which were contributed to the boundary-protecting films composed of Fe_xBy, Fe_2O_3 and B_2O_3 generated on the worn surfaces.

Many studies have shown that the combination of graphene and nano-particles not only enriched their original characteristics but also produced synergism and gave them new functions, which was very helpful in improving the tribological performance of graphene. Jia et al. (Ref 15) prepared calcium borate/graphene oxide (CB/GO) composites with a hydrothermal method. The GO nano-sheets uniformly surrounded the leaf-like CB and effectively inhibited the agglomeration and growth of CB. The tribological test results showed that the base oil with 0.5 wt.% CB/GO nano-composite had the best tribological properties, ascribed to the tribofilms containing C, O, B, Ca, and Fe generated on the worn surface. Yang et al. (Ref 16) prepared calcium borate/cellulose acetate-laurate (CB/CAL) nano-composite with a hydrothermal method and comparatively investigated the tribological properties of CB, CAL and CB/CAL nano-composite in PAO base oil. They found that the tribological properties of CB/CAL nano-composite superior to those of the single CB and CAL. CB and CAL exerted a synergistic effect during the friction process. The CB was uniformly dispersed in the CAL. The CB nano-particles mainly played the role of roller action. The CAL enhanced the dispersion stability of CB nano-particles. It reduced the agglomeration of CB nano-particles in the base oil, which promoted the formation of the oil film on the friction surfaces.

As a lubricant additive, graphene is easy to form a friction adsorption film and dual transfer membrane on the friction interface, which significantly improves the load capacity of the lubricant and the anti-wear ability of the friction pairs. In addition, graphene can improve the oxidation and decomposition temperature of lubricating oil and enhance the thermal conductivity ability of lubricating oil, which is beneficial to the heat dissipation of the cylinder and crankshaft of the engine (Ref 10, 12). Nano-borate has excellent extreme press and anti-wear properties, and borate has many ideal properties, including cleanliness, adaptive seal, anti-oxygen resistance and environmental friendly (Ref 12, 15, 16). The development of a multi-function lubricant additive composed of graphene and nano-borate can provide a feasible solution for the abnormal wear failure of a diesel engine under harsh conditions. However, graphene and borate are not dispersed in the base oil and are prone to agglomerate, which limits their extensive application in the field of lubricant additive (Ref 1, 12). Therefore, effectively preparing graphene and borate nano-composite with good dispersibility is the key to ensuring good friction reduction and wear resistance.

Dielectric barrier discharge plasma-assisted ball milling (DBDP-assisted ball milling) is a preparation method for nano-lubricant additive (Ref 17). DBDP-assisted ball milling has the characteristics of high efficiency, easy operation and low cost in the synergy of plasma and mechanical milling balls during the ball milling process. The nano-lubricant additive prepared by DBDP-assisted ball milling has the advantages of strong surface modification, good dispersion stability and antifriction properties. Ji et al. (Ref 18) prepared Cu nano-particles with stearic acid as surfaced modifier by DBDP-assisted ball milling for 5 h. They found that the surface-modified Cu nanoparticle has good dispersibility in lubricating oil and enhanced the tribological properties of lubricating oil.

In this investigation, extended graphite (EG) and potassium borate (PB) were used as raw materials to prepare a potassium borate/graphene (PB/GN) nano-composite lubricant additive with oleic acid serving as a surface modification by DBDP-assisted ball milling. FE-SEM, TEM, XRD, Raman, and FT-IR techniques were used to examine the morphology, composition, and structure of the PB/GN nano-composite. Using a pin-on-disk tribotester, the tribological characteristics of PB/GN nano-composite as lubricant additive in 500 N base oil were studied. The PB/GN nano-tribological composite's mechanism was investigated.

2. Material and Methods

2.1 Preparation of PB/GN Nano-composite

Expanded graphite (EG) exhibiting a 300 ml/g expansion rate was obtained from unexpanded graphite, which was purchased from Shanghai Yifang Graphite Co., Ltd. Potassium borate (PB), Oleic acid (OA) and 500 N base oil were purchased from Xilong Scientific Co., Ltd., Sinopharm Group and Zhuhai Jing Rui petrochemical co., Ltd. All chemical reagents are analytically pure. In this study, 500 N base oil was chosen because the base oil of marine cylinder oil FC5040 is 500 N. The prepared PB/GN nano-composite lubricant additive is mainly used for marine cylinder oil FC5040. Future work will comprehensively and systematically investigate the tribological properties of PB/GN nano-composite lubricant additive in marine cylinder oil FC5040.

The unexpanded graphite was heated to 1000 °C for 20 min, then cooled to room temperature to produce the expanded graphite (EG). The potassium borate/graphene (PB/GN) nano-composite powders were prepared from mixtures of powdered PB (2 g), EG (8 g), and oleic acid (500 mL) that were ball milled for 2 h, 6 h, 10 h, 15 h and 20 h in a plasma-assisted ball milling device (PBMS, South China University of Technology, China), described in the previous publication (Ref 19). The ethanol-mixed ball-milled nano-composite was heated to 50 °C, subjected to a 30 min ultrasonic treatment, and then subjected to a 15-min centrifugation procedure at a speed of 4500 rpm. The final products were nano-composite PB/GN materials.

2.2 Sliding Wear Testing

PB/GN nano-composite additive with different concentrations (0.03, 0.05 and 0.1 wt.%) were added to 500N base oil. The mixtures were treated by ultrasound for 45 min to make the additive uniformly dispersed in 500N base oil. During the current study, based on ASTM G181, the tribological performance of the base oil with different concentrations of additive was evaluated by a pin-on-disk tribotester (CFT-I, China), which was a pin-piston ring, $\varphi = 4$ mm, L = 20 mm; disk-cylinder liner, $\varphi = 29.5$ mm, h = 3.5 mm. The sliding wear of

the pin-on-disk was chosen to simulate the sliding wear of the piston ring-on-cylinder liner. The sliding wear with a linear velocity of the pin was 0.1 m/s, and a sliding distance of 10 mm was performed under a different contact load of 50–200 N for 60 min at 25–200 °C. The load 50–200 N was equivalent to 4–16 MPa (Ref 20). The applied load was chosen to simulate the nominal contact pressure between the piston ring and cylinder liner during combustion under actual marine diesel engine operation (Name of ship: Han Ren. Model of main engine: MAN B&W 6S42MC7. The nominal contact pressure between 4 and 16 MPa). The piston ring and cylinder liner were taken from a two-stroke marine diesel engine (MAN B&W 6S42MC7). The specific compositions of the piston ring and cylinder liner are detailed in Table 1. Before and after testing, the disk and pin were ultrasonically cleaned for 15 min and then dried in air. In order to reduce the experimental error, all tribological tests were carried out three times under the same experimental conditions.

2.3 Finite Element Analysis

The contact stress distribution has an important effect on the damage to the friction surface. Thus, the finite element method was used to calculate the substrate's elastoplastic stress and strain fields during sliding contact.

2.4 Structural Characterization

Various methods characterized the samples. Field emission scanning electron microscopy (FESEM, ZEISS VEO 18, Germany), high-resolution transmission electron microscope (HRTEM, TECNAI G230S-TWIN, Japan), Raman spectroscopy (HREvolution, HORIBA JobinYvon, France) and XRD (Mini Flex600, Japan) were used to characterize the microstructure and chemical composition of the sample. FT-IR (NICOLET IS10, The United States) was employed to confirm the chemical groups of the sample surface. X-ray photoelectron spectroscope (XPS, Thermo Fisher Scientific, USA) with AI K radiation excitation source were employed to investigate the composition and chemical states of the tribofilm on the worn surfaces of disks.

3. Results

3.1 Microstructure Evolution of PB/GN Nano-composite During Ball Milling

Figure 1 shows the SEM images of EG, PB and DBDP-assisted ball milled PB/GN nano-composite at different time. It can be seen from Fig. 1(a) that the surface of EG is smooth and has a good lamellar structure. PB are irregular particles exhibiting about 20–50 μm. After DBDP-assisted ball milling 2 h, a GN presenting a flat flake shape without obvious folds is obtained, most of the PB nano-particles are attached to the surface of GN, and a small part of PB is embedded into GN, as given in Fig. 1(c). For 6 h ball milling, the edge of GN shows an obvious step lamellar structure, but it is still thick, and the uneven distribution of PB nano-particles can be seen on the edge of GN, as given in Fig. 1(d). With further ball milling, more and more PB nano-particles are significantly refined to move from the edge of the GN and embed into GN. Meanwhile, GN is cracked and exfoliated, exhibiting a thinner yarn shape, more transparency and more folds at the edges, as given in Fig. 1(e). For 15 h ball milling, both a higher transparency of GN and more obvious folds appear in many places, indicating that the number of layers of GN significantly reduces, as given in Fig. 1(e). With further increasing the milling time to 20 h, as given in Fig. 1(g) and (h), the lamellar structure of GN exhibits a transparent tulle morphology due to obvious peeling off by DBDP-assisted ball milling, which indicates that EG during milling forms multilayer graphene. In addition, it can be seen from Fig. 1(h) that many PB nano-particles with about 10–50 nm size are loaded on GN. This is because a part of PB nano-particles is embedded into the layers of GN during the exfoliation process, which further accelerates the exfoliation of GN. From the exfoliation and refinement behavior of GN and PB, it can be attributed that the micro-zone heating effect generated by the plasma increases the interlayer distance of EG flakes and reduces the force between them simultaneously. Meanwhile, the shearing force generated by the balls in the milling tank makes EG flakes easy to shear. Coupled with the continuous embedding effect of PB nano-particles on EG flakes, GN is easier to exfoliate from the EG flakes. With the increase of milling time, the high-energy plasma produces a high-speed impact on the powders of EG and PB, which causes the powders to heat up quickly and produce a thermal explosion effect, accelerates the refinement of the powder, and forms PB/GN nano-composite.

To compare quantitatively the number of GN layers in PB/GN nano-composite powders prepared by different ball milling times. TEM was used to observe PB/GN nano-composite after DBDP-assisted ball milling for 10 h, 15 h and 20 h in Fig. 2. As can be seen from Fig. 2(a), when DBDP-assisted ball milling for 10 h (PM10h), GN is transparent and partially peeling, the surface presents a wavy morphology and multiple folds. The number of GN layers is about 20, as given in Fig. 2(b). When DBDP-assisted ball milling for 15 h (PM15h), GN exhibits more folds and transparency than that of PM10h, and the number of GN layers is about 10, as given in Fig. 2(c) and (d). For 20 h DBDP assisted ball milling (PM20h), GN shows transparent morphology and obvious folds, and the number of GN layers reduces to 8, as given in Fig. 2(e) and 2(f).

Figure 3 shows the XRD patterns of PB/GN composites at different ball milling times. The peak position of PB/GN composites did not change at different ball milling time. Both PB and C phases were detected in all samples after ball milling.

Table 1 Detailed material compositions of cylinder liner and piston ring

Main elements, wt.%	Fe	C	Si	S	P	Mn	AI	Ni	Cr	Mo	Cu	B
cylinder liner	92.01	3.58	1.80	0.07	0.28	0.67	0.003	0.46	0.45	0.44	0.21	0.005
piston ring	89.02	4.23	4.21	0.01	0.23	0.92	0.004	0.53	0.16	0.55	0.13	0.002

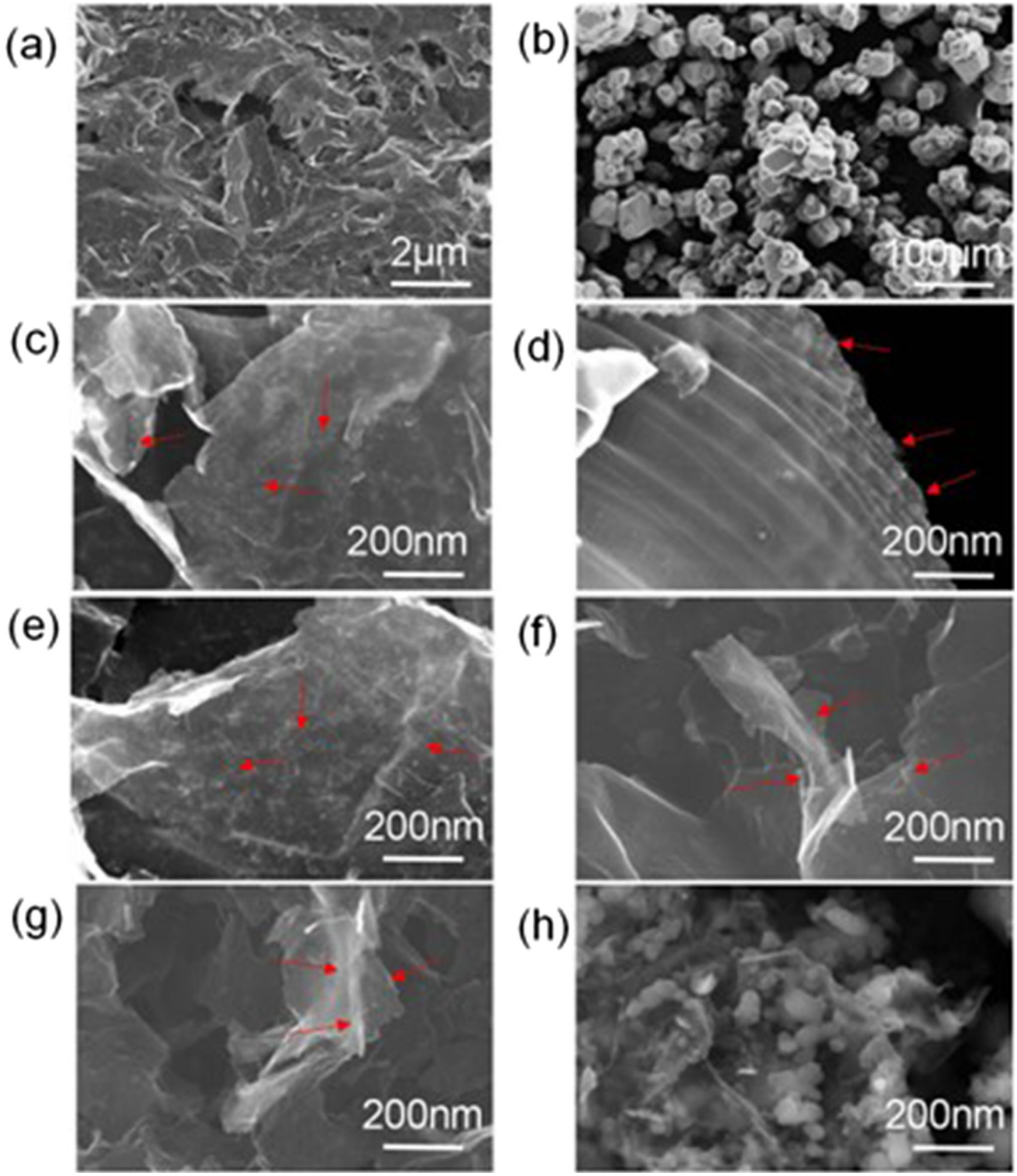

Fig. 1 SEM images of (a) EG, (b) PB and (c-h) PB/GN composites after DBDP assisted ball milling for 2 h, 6 h, 10 h, 15 h, 20 h, (c) PM2h, (d) PM6h, (e) PM10h, (f)PM15h, (g) (h) PM20h

The PB (022) crystal plane and C (002) crystal plane diffraction peaks are the strongest. The later diffraction peak gradually weakened with the increase of ball milling time. The peak strength of the C (002) crystal plane decreased most obviously when the ball milling time was 6 h (PM6h), which indicates that EG is gradually peeled and refined with the prolonging of ball milling. The lamellar structure of GN is destroyed. With the increase of ball milling time, the intensity of the PB phase peak decreases obviously before PM6h and does not change obviously after PM6h. It is attributed that a combination of the heating effect of the plasma and the mechanical energy of steel balls in the ball tank created synergies. At the beginning of the

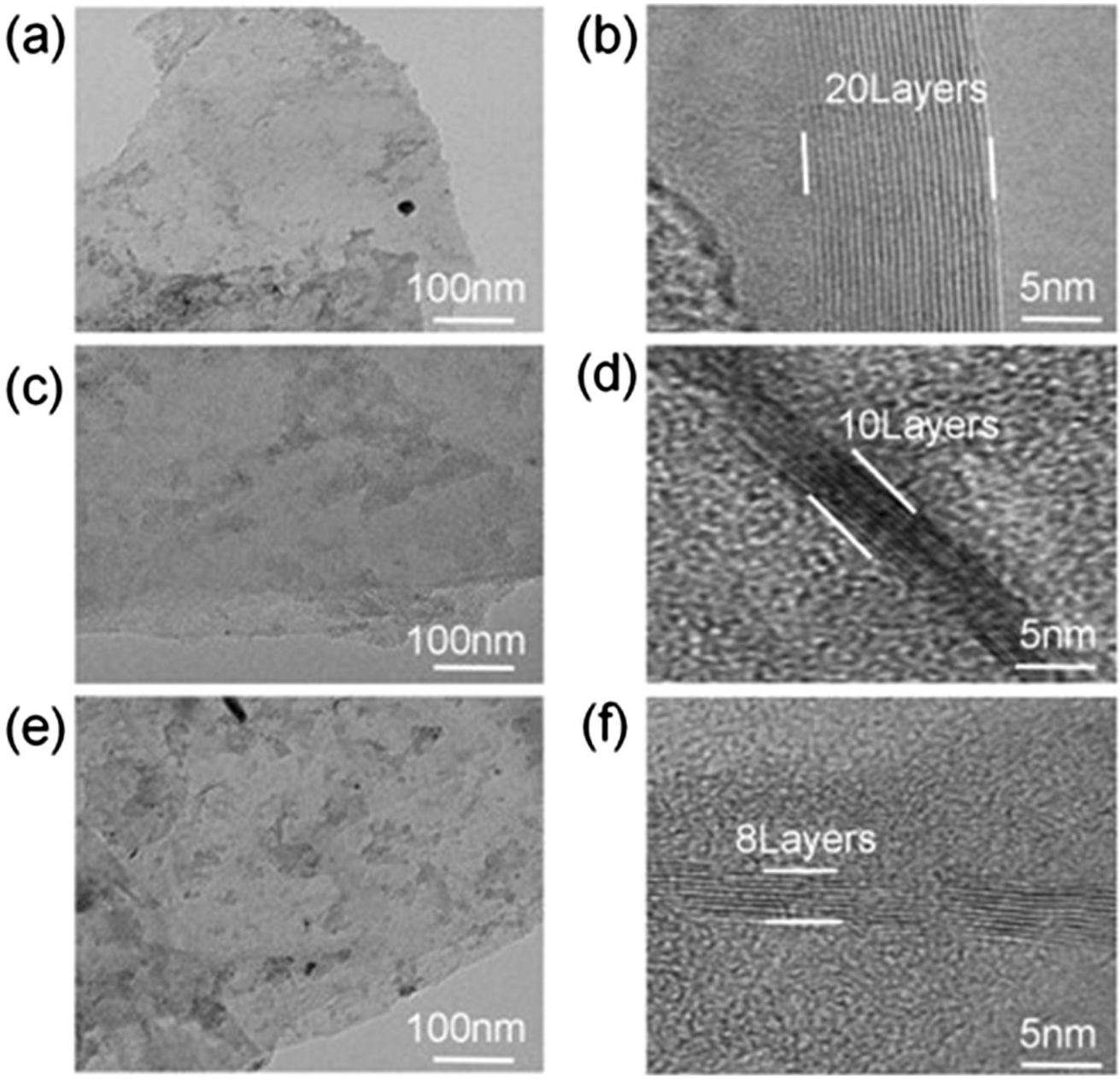

Fig. 2 TEM images of PB/GN composites when DBDP assisted ball milling for10h, 15 h, 20 h. (a) (b) PM10h, (c) (d) PM15h, (e) (f) PM20h

ball milling, the great impact force from the steel balls produces a dramatic change in the internal structure of PB particles. It forms a large number of defects, which causes the particle size to change obviously. However, when achieving a certain ball milling time, the mechanical refining effect of steel balls on PB particles was limited, and the thermal explosion effect of plasma played a dominant role in further refining PB nano-particles. Therefore, PB's particle size and lattice distortion changed little, and the diffraction peak height and width did not change after PM6h.

The Raman patterns of PB/GN composites at different ball milling times for 2 h (PM 2 h), 6 h (PM 6 h), 10 h (PM 10 h), 15 h (PM 15 h), 20 h (PM 20 h) are shown in Fig. 4. The peaks at 1350 cm^{-1} is attributed to the disordered carbon while that at 1580 cm^{-1} is ascribed to the characteristic peak of the in-plane vibration of a layer of sp^2 carbon atoms (Ref 21-23). The D and G band intensities (I_D/I_G) ratio, defining the graphitization degree of carbon materials (Ref 24), in the spectrum obtained from the PM2h sample was approximately 0.13. However, this value increased to 0.24 in the spectra of the PM20 h samples. These results are ascribed to the thermal explosion effect of the micro-zone of the plasma, which would be expected to accelerate mechanical peeling and thermal expansion and decrease the number of layers in the EG during ball milling. This result is in good agreement with TEM results in Fig. 2. In addition, the position of the 2D band shifted gradually to the left with the increase of milling time, which shifted from 2715 cm^{-1} of PM 2 h to 2688 cm^{-1} of PM 20 h, also indicating that the number of layers of EG is decreasing (Ref 25). From PM2h to PM6h, the 2D peak offset is the largest, which is consistent with the result of XRD in Fig. 3. Therefore, PM 20 PB/GN nano-composite being additive will

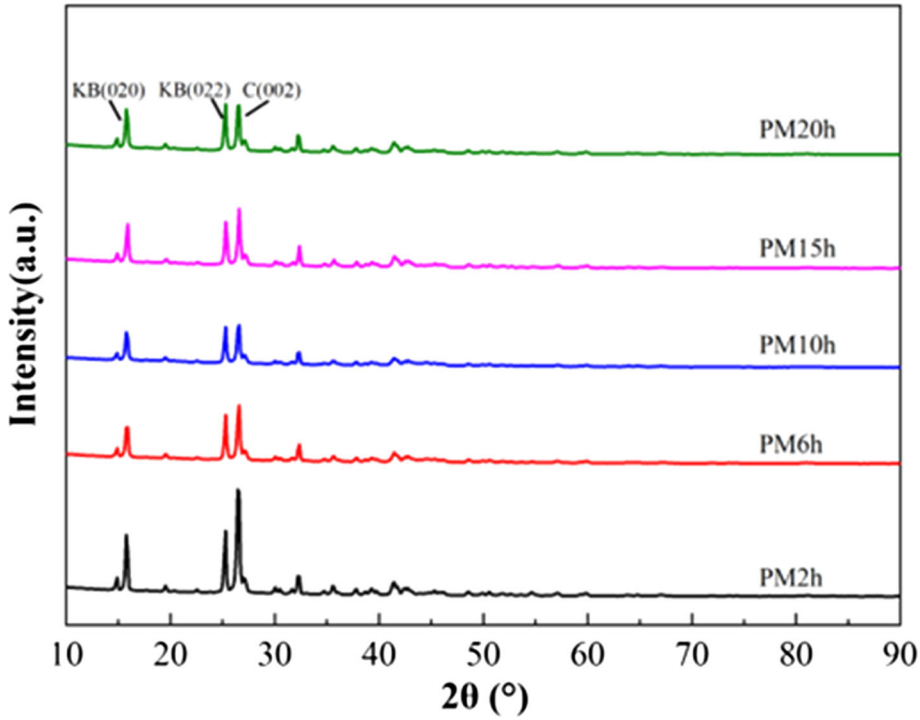

Fig. 3 XRD patterns of PB/GN composites when DBDP assisted ball milling for 2 h (PM2h), 6 h (PM6h), 10 h (PM10h), 15 h (PM15h), 20 h (PM20h)

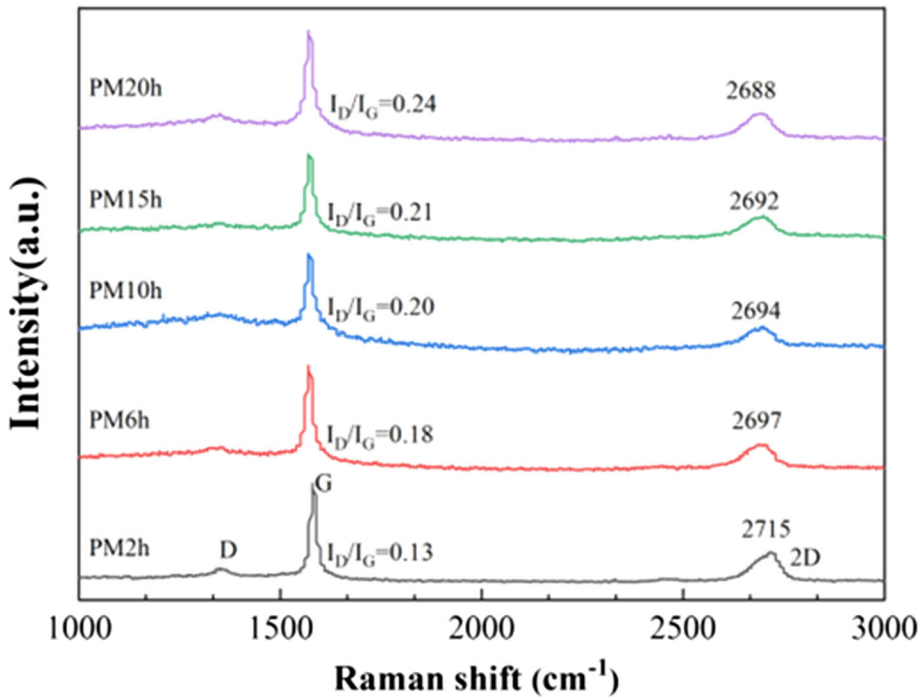

Fig. 4 Raman patterns of PB/GN composites when DBDP assisted ball milling for 2 h (PM2h), 6 h (PM6h), 10 h (PM10h), 15 h (PM15h), 20 h (PM20h)

be chosen to add into 500N base oil to investigate its tribological properties in next section further (Fig. 4).

Figure 5 shows the FT-IR spectra of PB, EG, OA (oleic acid) and PB/GN nano-composite power when DBDP-assisted ball milling for 20 h (PM20h). In the spectrum of PB, the band at 3440 cm^{-1} belongs to the stretching vibration of the O–H group. In contrast, those at 1390, 1063 and 894 cm^{-1} are ascribed to the asymmetric stretching of B(3)-O, the asymmetric and symmetric stretching of B(4)-O, respectively (Ref 12, 26). In the spectrum of EG, the bands at 3440 and 2360 cm^{-1}

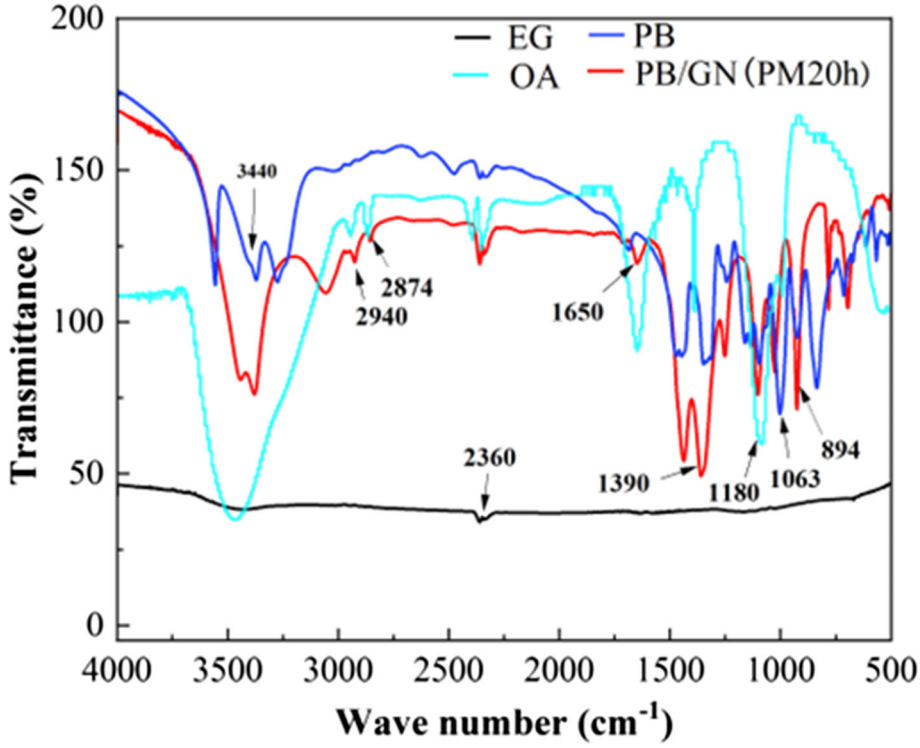

Fig. 5 FT-IR spectra of EG, PB and PB/GN composites when DBDP assisted ball milling for 20 h (PM20h)

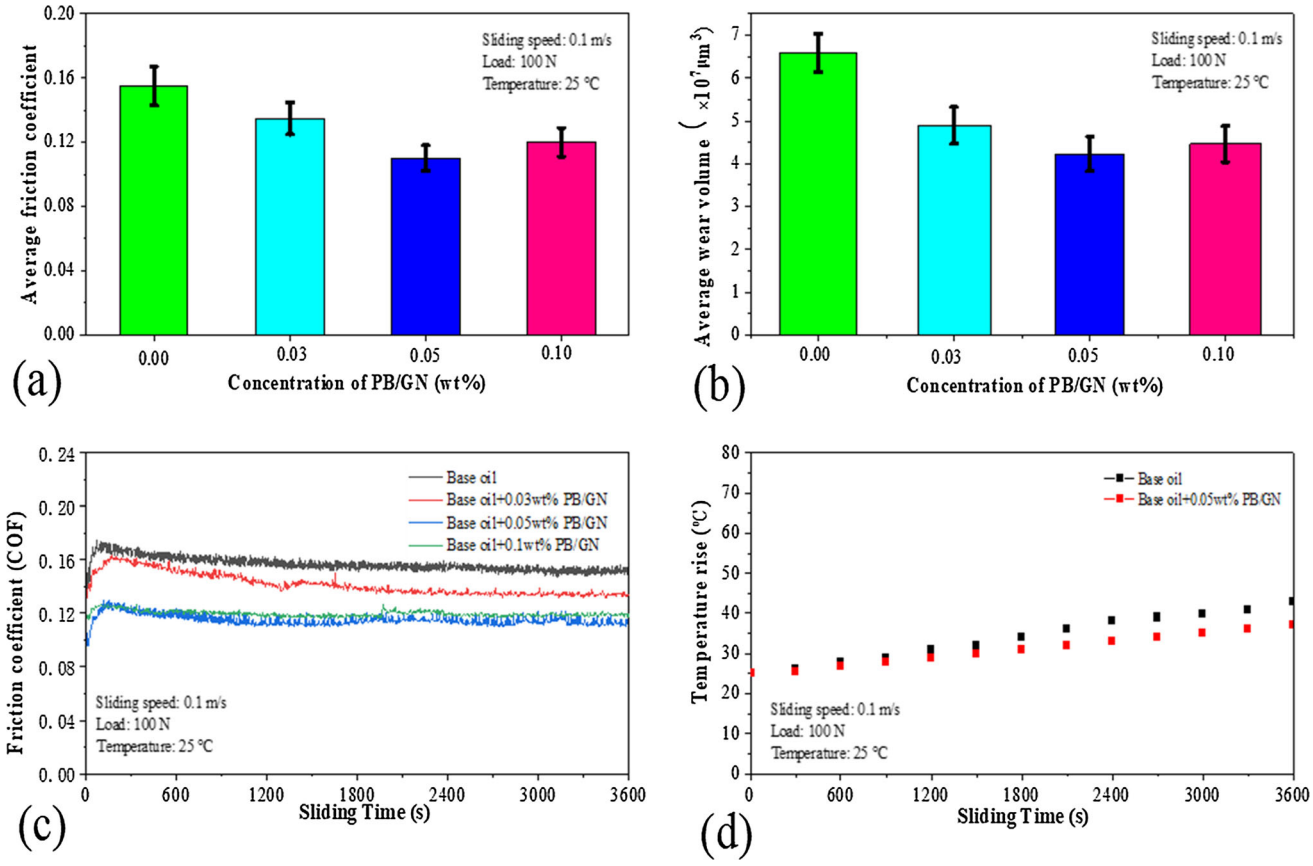

Fig. 6 Average friction coefficient (a) and average wear volume (b) of disks lubricated by base oil with different concentrations of PB/GN additive; Variations of friction coefficient (c) and temperature rise (d) with sliding time of disks lubricated by base oil with different concentrations of PB/GN additive

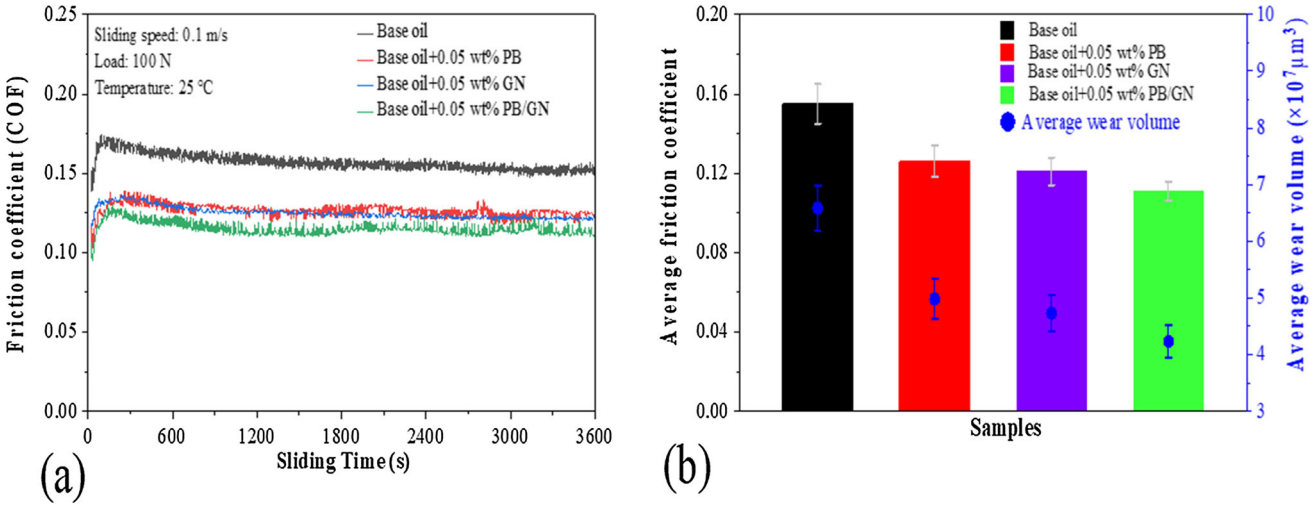

Fig. 7 The effect of different additive on tribological properties of 500 N base oil, (a) friction coefficient, (b) average friction coefficient and average wear volume

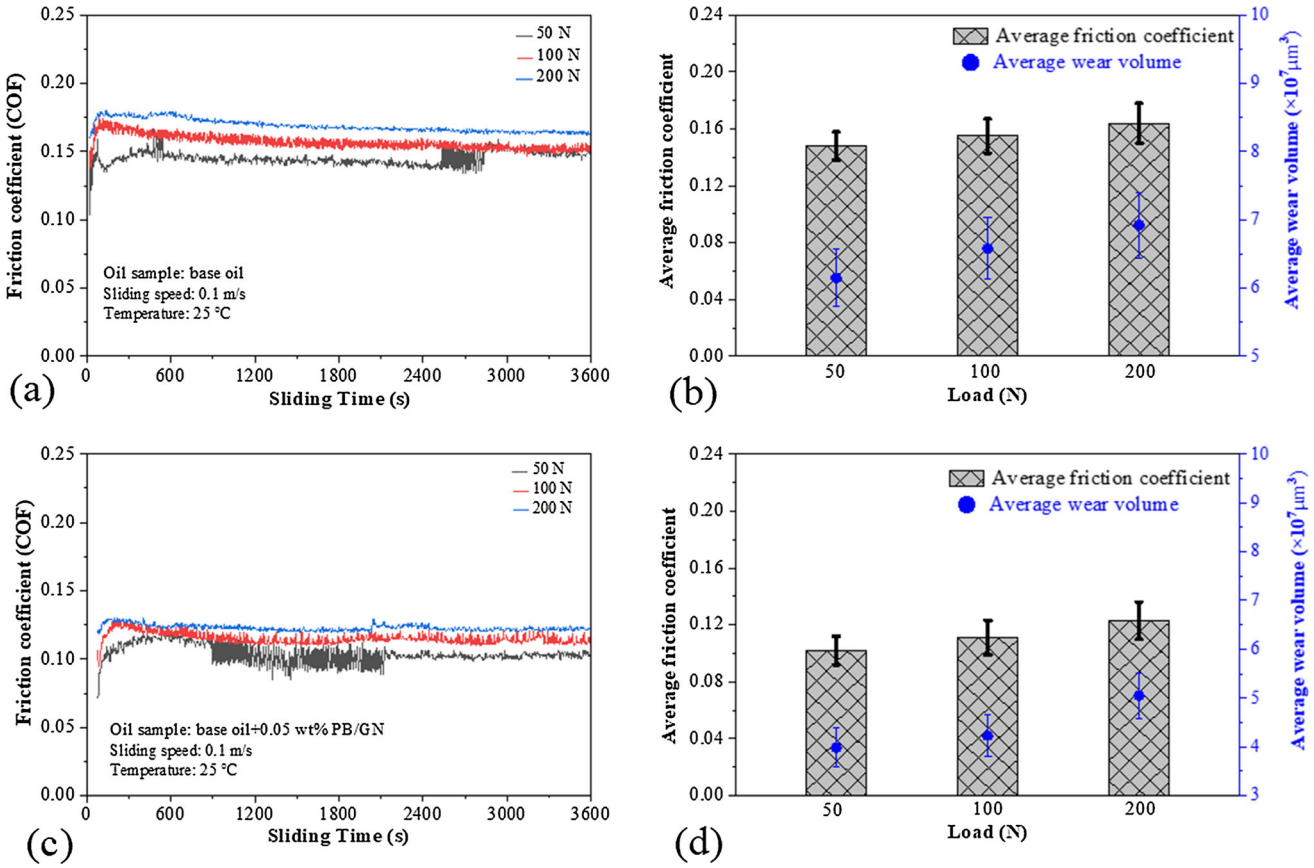

Fig. 8 The effect of different test loads on tribological properties of base oil (a) (b) and base oil with 0.05 wt.% PB/GN additive (c) (d)

are attributed to the stretching vibration to the O–H group and absorption peak of carbon dioxide (Ref 27). In the PB/GN nano-composite power spectrum of PM20h, the peaks at 2940 cm^{-1} and 2874 cm^{-1} correspond to the asymmetric and symmetric stretch vibration of $–CH_2$, respectively (Ref 28). The peak at 1650 cm^{-1} belongs to the C=C of OA (Ref 15). The band at 1180 and 1390 cm^{-1} are assigned to the C-O stretching vibration and C-OH stretching vibration of OA, respectively (Ref 15). The characteristic peaks of OA are distinctly presented in the spectrum of PB/GN nano-composite power, which indicates that OA had chemically modified the surface of PB/GN nano-composite power after PM20h. During DBDP-assisted ball milling, the plasma makes some high molecular polymers more prone to bonds broken and polymerization (Ref 29). At the same time, the highly active particles (ions, electrons, excited atoms and molecules, free radicals, etc.) of plasma were easily adsorbed with PB/GN powder, resulting in the improvement of the surface activity of the PB/GN powder.

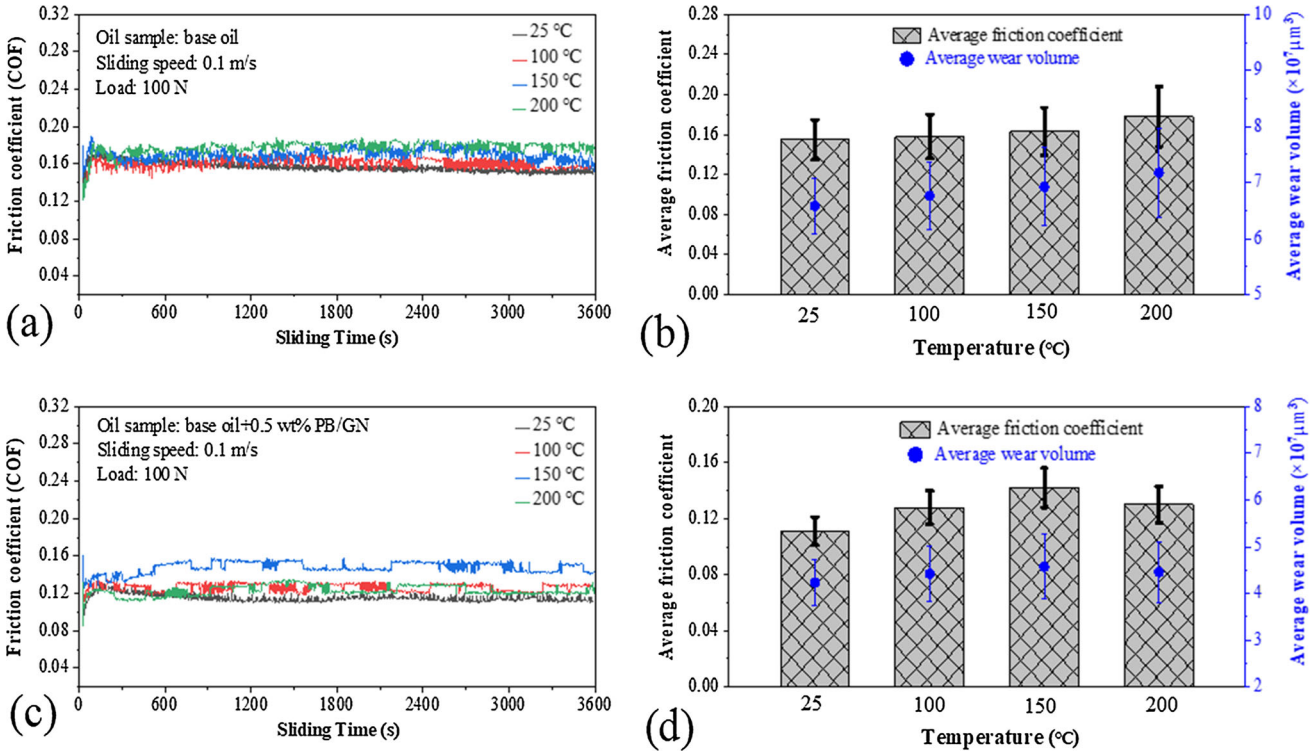

Fig. 9 The effect of different test temperature on tribological properties of base oil (a) (b) and base oil with 0.05 wt.% PB/GN additive (c) (d)

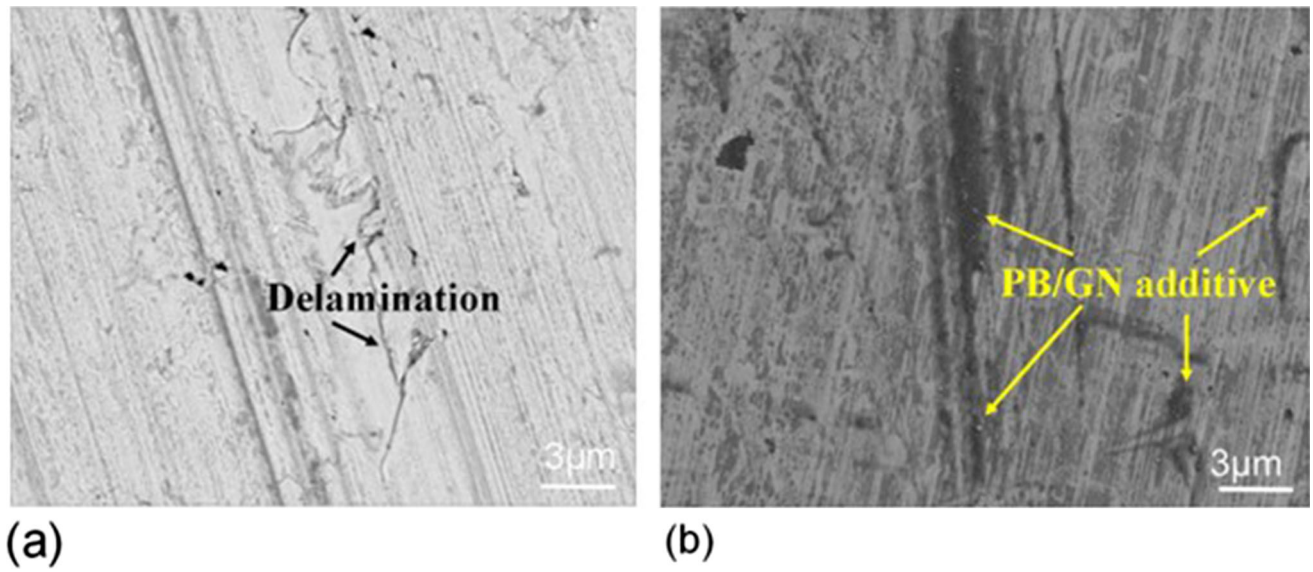

Fig. 10 Typical back-scattered electron image showing the worn surface of disks lubricated by different lubricants: (a) base oil, (b) base oi with 0.05 wt.% PB/GN additive

Meanwhile, the fresh surface and many defects introduced by ball milling further enhanced the activity of the PB/GN powder. OA, as a surface modifier of PB/GN powder in the ball milling process, the bonds of the organic functional groups (-CH_2, C=C, C-O and C–OH) of OA were broken under the action of plasma. The organic functional groups were adsorbed and polymerized on the surface of the high-activity powder, and thus the in-situ surface modification of the PB/GN powder was realized.

3.2 Tribological Properties of PB/GN Nano-composite as Lubricant Additive

3.2.1 Improvement of Wear and Friction by PB/GN Nano-composite Additive. In this section, PB/GN nano-composite by DBDP-assisted ball milling for 20 h (PM20h) was chosen further to investigate its tribological properties as lubrication oil additive. Here, PB/GN nano-composite as additive with different concentrations of 0.03, 0.05 and 0.10

wt.% were added to 500N base oil. The sliding wear performance of PB/GN nano-composite additive in 500N base oil with different concentrations was investigated under a different contact load of 50–200 N for 60 min at 25–200 °C.

Figure 6(a) and (b) shows the dependence of the friction coefficient and average wear volume of 500N base oil with different PB/GN additive (PM20h) content on the applied load. PB/GN additive led to apparent wear and friction performance improvements, as indicated by the lower friction coefficient and the lower average wear volume than the pure base oil. The friction coefficient and average wear volume were reduced obviously when the concentration of PB/GN additive was increased from 0 to 0.05 wt.%. This is because PB/GN additive enter the friction interface and reduce wear damage when the concentration increased from 0.05 to 0.1 wt.%, the friction coefficient and average wear volume of the base oil with 0.10 wt.% PB/GN additive higher than the base oil with 0.05 wt.% PB/GN additive. This might attribute to the fact that the PB/GN additive did not disperse uniformly and aggregated in the oil when the concentration was 0.10 wt.%, leading to poor anti-friction performance. Thus, the 500 N base oil with 0.05 wt.% PB/GN additive exhibits the best wear and friction behavior, which reduces friction coefficient and average wear volume by 29.1 and 35.8% compared with the pure base oil, respectively. Therefore, the PB/GN additive concentration plays an important role in the basic oil's tribological performance during sliding wear. Figure 6(c) and (d) shows variations of friction coefficient and temperature rise with the sliding time of disks lubricated by base oil with the different concentrations of PB/GN additive. As shown in Fig. 6(c), with the increase of sliding time, the friction coefficient of base oil and base oil with different additive contents showed a slow decline because in the friction process, the friction generated heat, the oil temperature increased, the oil viscosity decreased, and friction coefficient decreased. Figure 6(d) shows the temperature rise of the base oil and the base oil with 0.05 wt.% PB/GN additive increased with sliding time. After sliding for one hour, the temperature of the pure base oil increased by 18 °C, and that of the base oil with 0.05 wt.% PB/GN additive increased by 12 °C. The temperature rise of the base oil with 0.05wt.% PB/GN additive was smaller than that of the pure base oil. This indicated that part of the friction-induced heat could be carried away by PB/GN additive, which led to decreased friction and wears, and reaffirms that the anti-friction and anti-wear properties of the base oil with 0.05 wt.% PB/GN additive was better than pure base oil.

Figure 7 shows the friction coefficient, average friction coefficient and average wear volume of the three additive under an applied load of 100 N at a sliding speed of 0.1 m/s and test temperature of 25 °C. The curves reveal that the average friction coefficient and wear volume of PB/GN additive were lower than that of PB additive and GN additive, which suggested that the synergistic effect of PB additive and GN additive enhanced the anti-friction and anti-wear properties of PB/GN nano-composite additive.

Figure 8 shows the effect of different test loads on the tribological properties of base oil and base oil with 0.05 wt.%

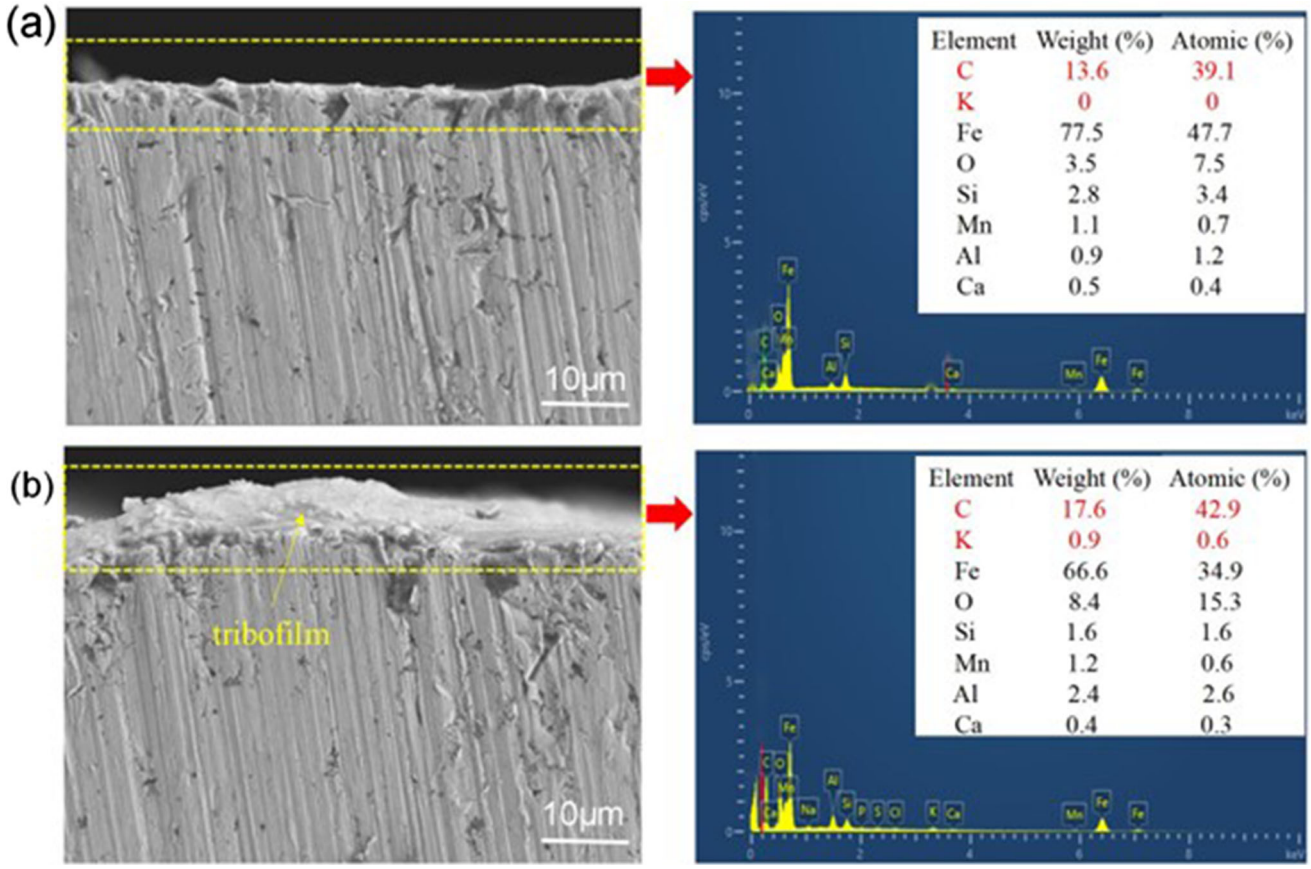

Fig. 11 EDS mapping of tribofilm formed on the cross section of the disks lubricated by different lubricants: (a) base oil, (b) base oil with 0.05 wt.% PB/GN additive

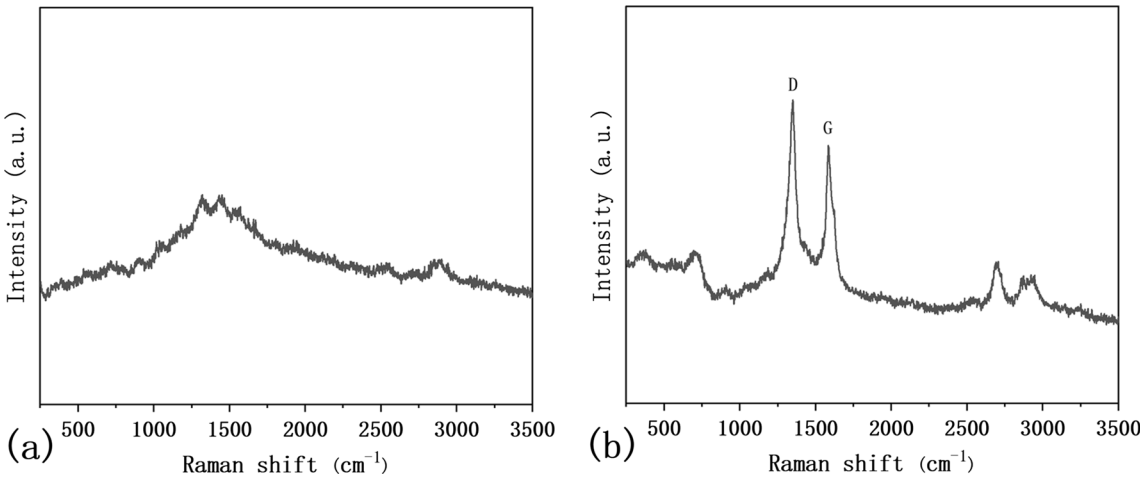

Fig. 12 Raman spectra of the worn surfaces of disks lubricated by (a) base oil, (b) base oil with 0.05 wt.% PB/GN additive (PM20h)

PB/GN additive. For both base oil and base oil with 0.05 wt.% PB/GN additive, the average friction coefficient and average wear volume increased with the load from 50 to 200 N. It can be seen that the average friction coefficient and average wear volume of base oil with 0.05 wt.% PB/GN additive under various loads were lower than that of the base oil, which indicated that PB/GN additive has good anti-friction and anti-wear properties.

Figure 9 shows the effect of different test temperature on the tribological properties of base oil and base oil with 0.05 wt.% PB/GN additive. It can be seen from Fig. 9(b) that the average friction coefficient of the base oil was around 0.155 and 0.178 at 25 °C and 200 °C, respectively. The average friction coefficient and average wear volume of the base oil increased gradually with the rising temperature. This might be attributable to the carbonization of 500 N base oil and the amorphous carbon and asphaltene products. These deteriorative products were hard, which might scratch the contact surface during friction, and thus lead to increased average friction coefficient and average wear volume. It can be seen from Fig. 9(d) that the average friction coefficient of the base oil with 0.05 wt.% PB/GN additive was around 0.111 and 0.130 at 25 and 200 °C, respectively. The average friction coefficient and average wear volume of the base oil with 0.05 wt.% PB/GN additive decreased than that of the pure base oil. This indicated that adding PB/GN additive could effectively improve the tribological properties of base oil at different temperatures. Compared to pure base oil, adding PB/GN additive to base oil could significantly decrease the average friction coefficient and average wear volume when the temperature reached 200 °C, average friction coefficient and average wear volume reduced by 27 and 38%, respectively. This might be due to PB and GN additive's synergistic effect. Part of the friction-induced heat could be carried away by the GN additive, which might moderately slow the temperature rise of the contact surface. Meanwhile, the PB additive and the GN additive could form a deposited layer at elevated temperature during friction.

3.2.2 Microstructural Evolution of the Worn Surface. As described above, PB/GN additive can effectively increase the anti-friction and anti-wear properties of 500N base oil. Now, we discuss the mechanisms of PB/GN additive on anti-friction and anti-wear properties and the microstructural evolution of the sliding worn interfaces under the contact load of 100 N for 60 min at 25 °C.

In general, different sliding wear behaviors are displayed by the microstructural evolution of the sliding interfaces. A significant difference in the worn surfaces of the steel disks lubricated by base oil without and with 0.05 wt.%. The SEM images in Fig. 10 revealed PB/GN additive (PM20 h). While the monolithic base oil exhibited severe adhesive wear and delamination wear (Fig. 10a), the extreme wear was significantly relieved with increasing PB/GN additive content, and a trilayer containing PB/GN additive formed on the sliding surface as given in Fig. 10(b). Therefore, PB/GN additive containing many GN platelets scattered at the contact interface and hence direct metal-to-metal contact was hindered, which might play an important role in improving the microstructural evolution of the worn surface.

To understand the wear and lubrication mechanism, the EDS mapping of tribofilm formed on the cross-section of the disks lubricated by different lubricants are shown in Fig. 11. The corresponding EDS mapping clearly shows distinct element content. The content of carbon and potassium in the tribo-interface increased when the disks were lubricated by base oi with 0.05 wt.% PB/GN additive indicated that the PB/GN additive enter the tribo-interface and form a protective film. The formation of the tribofilm helps delay or prevent adhesive wear and delamination wear, as present in Fig. 10(a).

To investigate the formation and microstructure evolution of protective films in the tribo-interface, Raman spectra of the tribo-interface lubricated by base oil and base oil with 0.05 wt.% PB/GN additive (PM20h) is shown in Fig. 12. It indicates that several strong graphene peaks can be observed on the worn surface lubricated by base oil with 0.05 wt.% PB/GN additive, but is not observed in the base oil sample. It has been well established that the peak at 1583 and 1350 cm^{-1} are attributed to the G band of typical crystalline carbon and the stretching vibration of D in graphene (Ref 30). The peak at 619 cm^{-1} is assigned to the bending model of trigonal and tetrahedral boron (Ref 13). These findings indicate that PB/GN nano-composite additive entered the interface of the friction pairs and formed GN platelets undergoing slippage on the

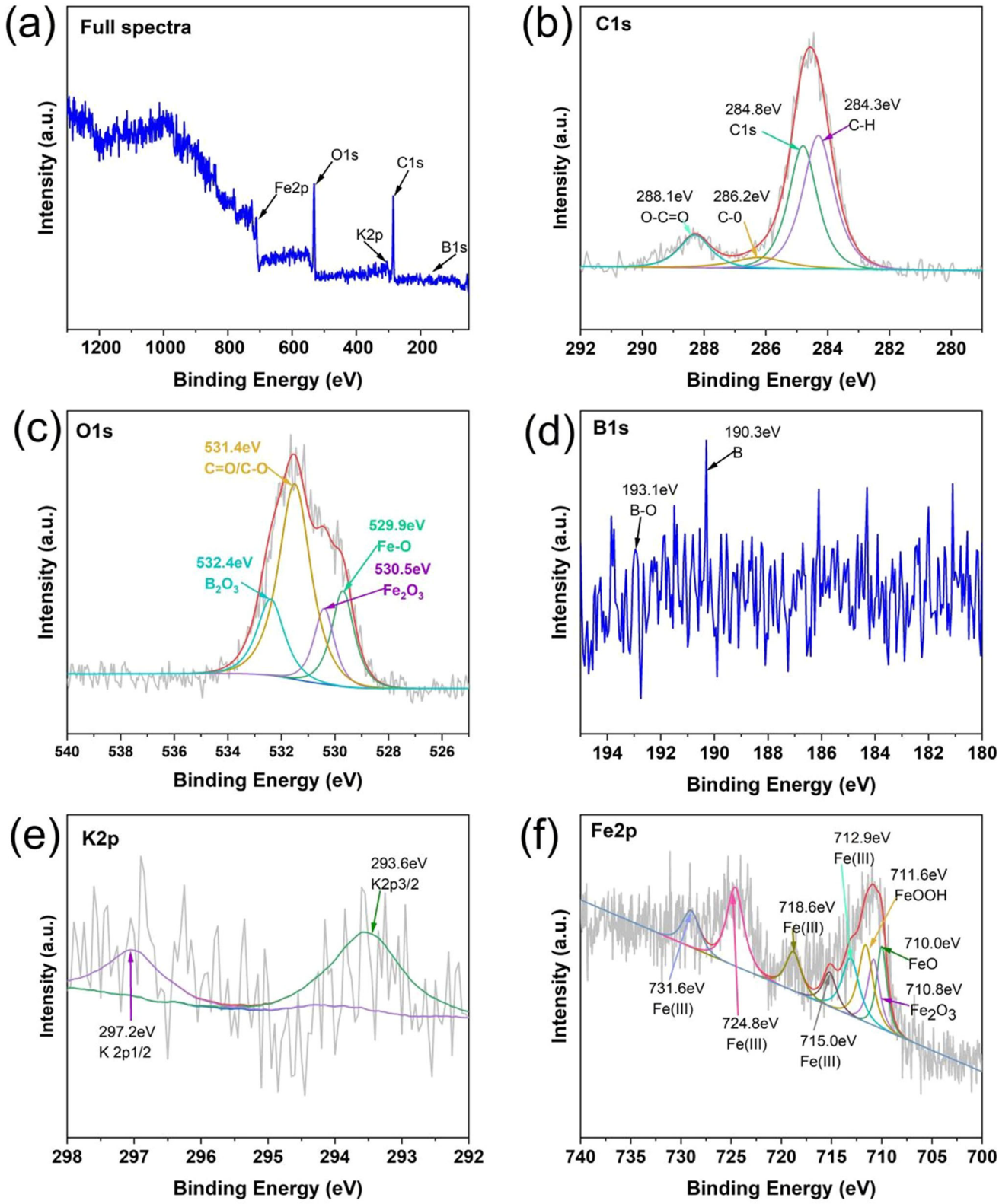

Fig. 13 XPS spectra of the worn surface of disk lubricated by based oil with 0.05 wt.% PB/GN additive (PM20h)

tribo-interface during sliding wear. As well known, GN-containing protective films are beneficial for wear properties because of their special laminated structure and remarkable super lubricating properties, which could lower the friction force and improve anti-friction properties.

In addition, XPS spectra of the tribo-interface lubricated by base oil with 0.05 wt.% PB/GN nano-composite additive are shown in Fig. 13. The characteristic peak of C1s, O1s, B1s, K2p and Fe2p were detected from the survey scan XPS spectra on the worn surfaces, as given in Fig. 13(a). Figure 13(b) presents the

XPS spectra of C1s on the worn surface, showing that the peaks at 284.3, 284.8, 286.2, and 288.1 eV belong to C-H, C–C/C=C, C-O, and O-C=O bonds, respectively (Ref 12, 15, 31). Combining the analyses of Raman spectra (Fig. 12b), the presence of the C–C/C=C bands of 284.8 eV indicates that graphene entered into the interface of friction pairs and formed tribofilms (Ref 11). The O 1 s data shown in Fig. 13(c) confirm that oxygen was present on the surface in three states, which include a strong peak at 531.4 eV related to C = O/C-O and two peaks at 529.9, 530.5, and 532.4 eV that are attributed to Fe-O and B-O groups (Ref 17). Figure 13(d) presents the XPS spectra of B1s on the worn surface, the peaks at 190.3 and 193.1 eV are associated with B and B-O, respectively. A combination of the peak of B1s appeared at 193.1 eV, and the binding energy of O1s at 532.4 eV is assigned to B2O3 (Ref 12). The two minor peaks at binding energies of 293.6 and 297.2 eV are associated with the K2p1/2 and K2p3/2, as shown in Fig. 13(e) (Ref 32). Figure 13(f) presents the XPS spectra of Fe2p on the worn surface. The peaks that appeared at 710.0, 710.8 and 711.6 eV relate to the binding energies of O1s at 529.9, 530.5 and 531.4 eV, attributing to FeO, Fe2O3 and FeOOH (Ref 12, 30, 33). Therefore, XPS results indicate a tribo-chemical reaction between PB/GN nano-composite additive and steel disk surface occurred during the wear process. A physical adsorption membrane and tribo-chemical film were generated to prevent direct contact between the inner surfaces of the friction pairs.

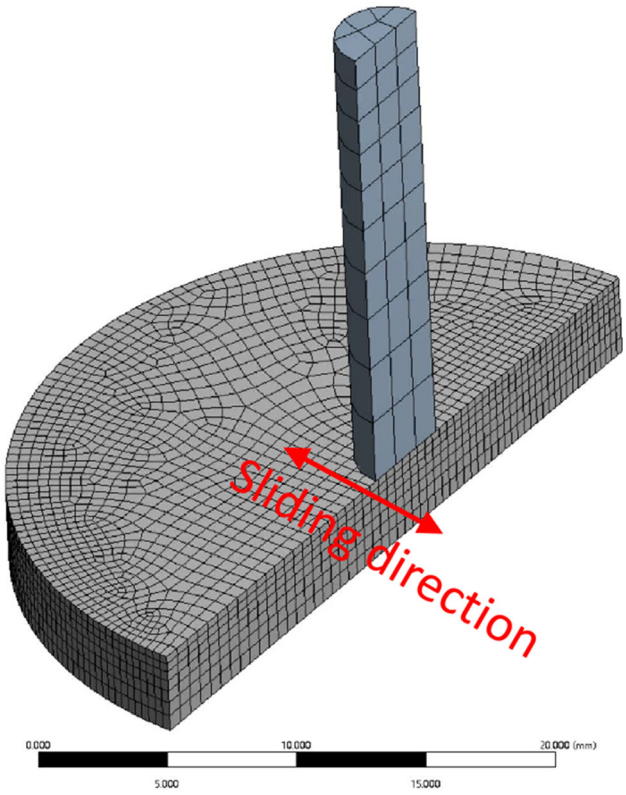

Fig. 14 The finite element mesh used to simulate sliding contact. Calculations of stress fields were set in the worn surface of the disk-cylinder liner nearest to the middle of the pin and perpendicular to the sliding direction

3.2.3 Tribological Mechanism of PB/GN Nano-composite additive. The high surface stress localized for metal sliding contacts plays a key role in the damage to the worn surface. Thus, finite element analysis was used to calculate the substrate's elastoplastic stress and strain fields during sliding contact. The finite element mesh is depicted in Fig. 14, where the gray color represents the disk-cylinder liner, and the blue Colour represents the pin-piston ring. The disk-cylinder liner and pin-piston ring were treated as isotropic elastic materials with Young's modulus and Poisson's ratio of E = 110 GPa, ν = 0.25, respectively. In meshing mesh, as given in Fig. 14, the overall meshing defeature size of the disk-cylinder liner was 0.02 mm.

In Fig. 15, Von Mises stress contour graphs are shown for sliding wear lubricated by base oil (f = 0.16) and base oil with 0.05 wt.% PB/GN additive (f = 0.11) samples in the worn surface that is closest to the middle of the pin and perpendicular to the sliding direction. The arrows in Fig. 15 show that the peak stress values of 6.6 MPa, which are situated at the boundary of both sides of the friction pair, are present in both the base oil and the base oil with 0.05 wt.% PB/GN additive samples. But the location of the peak stress values is where the base oil and base oil with 0.05 wt.% PB/GN additive samples

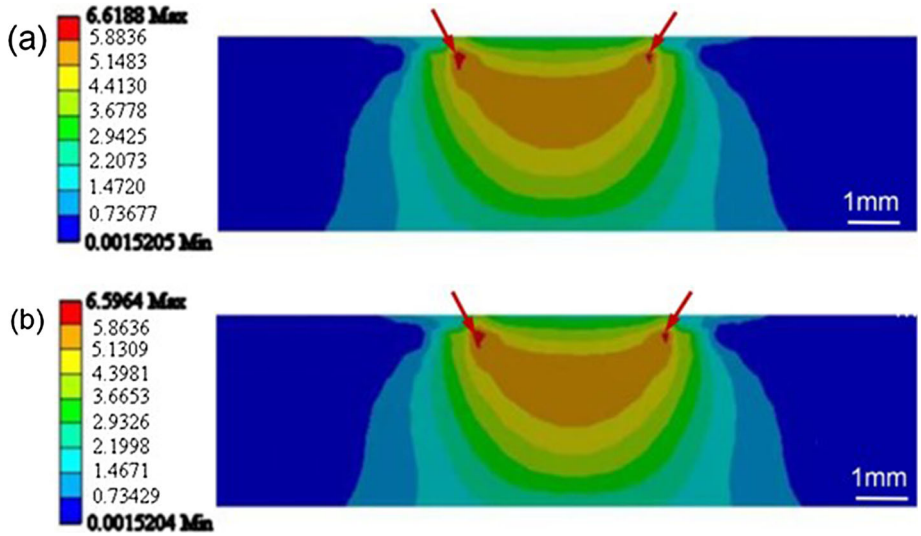

Fig. 15 Elasto-plastic finite element results for sliding friction showing von Mises stress contours (MPa): (a) base oil, (b) base oi with 0.05 wt.% PB/GN additive

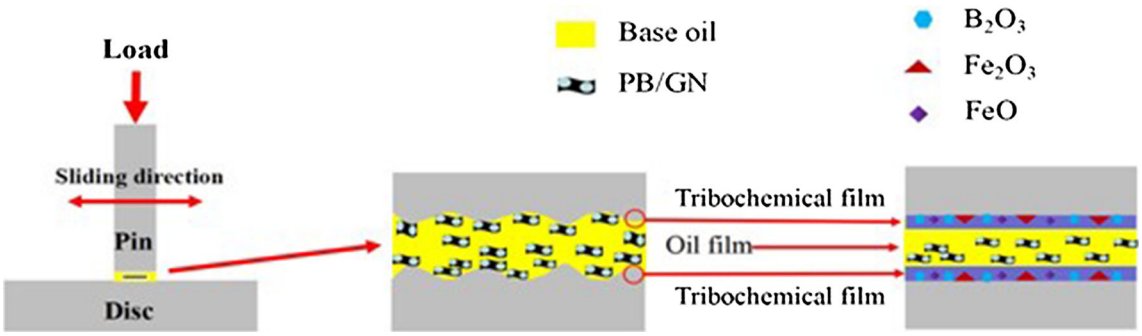

Fig. 16 The schematic diagram of tribological mechanism for base oil with PB/GN additive

differ the most noticeably from one another. Due to the latter sample's lower friction coefficient than the earlier sample, the peak stress is 50 m below the worn surface, whereas a greater friction coefficient causes the peak stress to be closer to the topmost surface. According to Fig. 10, if delamination wear and a larger wear track are visible, the peak stresses close to the worn surface are more likely to harm the uppermost worn surface. In contrast, the smeared PB/GN lubricant could shift the location of the peak stress deep below the worn surface and prevent significant wear damage at the highest worn surface, which prevented adhesion and delamination wear.

PB/GN nano-composite, as lubricating oil additive, can effectively improve the tribological properties of base oil. Based on the above analyses, the tribological mechanism of PB/GN nano-composite was proposed, which is presented in Fig. 16. In the process of preparing PB/GN nano-composite powder by DBDP-assisted ball milling, the highly active particles (ions, electrons, excited atoms and molecules, free radicals, etc.) of the plasma can easily adsorbed on the PB/GN nano-composite powder and caused the improvement of the surface activity of the powder. In addition, the fresh surface and many defects introduced by DBDP-assisted ball milling further enhanced the activity of the PB/GN nano-composite powder, which promoted diffusion, phase transitions, and chemical reactions easier. In the early stage of friction, PB/GN nano-composite entered and absorbed the friction interface, forming a layer of physical adsorption membrane full of PB and GN, which prevented direct metal-to-metal contact between the friction interfaces and reduced friction and wear. As sliding continued, the surface temperature of the friction pairs increased, and tribochemical reactions occurred between the PB/GN nano-composite and the worn surface. A layer of tribochemical film composed of C, FeO, Fe_2O_3 and B_2O_3 formed on the friction surface, effectively preventing direct contact between the friction pairs' metal surfaces and reducing wear and friction. Meanwhile, the graphene accelerated the transfer of heat caused by friction, which led to decreased friction and wears. Therefore, the synergy of PB and GN greatly enhanced the tribological performances of base oil.

4. Conclusions

PB/GN nano-composite was prepared and used to improve the tribological performances of the 500N base oil by DBDP-assisted ball milling. Tribological tests were adopted to explore the tribological performances of PB/GN nano-composite. The tribological mechanism of PB/GN nano-composite in base oil was proposed. The following conclusions can be drawn.

(1) PB/GN nano-composite was prepared by DBDP-assisted ball milling for 20 h, the PB nano-particles with about 10–50 nm size were ununiformly distributed on GN platelets surface containing about 8 layers, and GN wrapped some PB nano-particles. The functional groups of oleic acid (-CH_2, C-O, C-OH and C=C) were successfully grafted onto PB/GN nano-composite surfaces.
(2) PB/GN nano-composite additive can significantly enhance the tribological performances of 500N base oil. The friction-reducing and anti-wear performances of base oil increased by 29.1% and 35.8% after adding 0.05 wt.% PB/GN nano-composite additive under the load of 100 N and the temperature of 25 °C.
(3) The finite element analysis showed that PB/GN nano-composite additive changed the maximum contact stress distribution position in the tribo-interface. When the pin on disk friction pair is lubricated by base oil with 0.05 wt.% PB/GN nano-composite additive, the distance of the maximum contact stress to the tribo-interface increased, and the wear decreased.
(4) The tribological mechanism of PB/GN nano-composite indicated that the tribochemical films of C, FeO, Fe_2O_3 and B_2O_3 were generated on the friction surface. These tribofilms effectively prevented direct metal-to-metal contact between metal interfaces and reduced friction and wear.

Acknowledgments

This work was financially supported by National Natural Science Foundation of China (51779103), Natural Science Foundation of Fujian Province (2021J01848, 2020J01687), Open Research Fund of Fujian Shipping Research Institute of Jimei University, Natural Science Foundation of Guangxi Province (2018GXNSFAA138157), Science and technology base and talent special project of Guangxi Province (2018AD19011), Beibu Gulf University 2018 school-level research project (2018KYQD22, 2019JGZ015), Guangxi First-class Discipline of Shipbuilding and Ocean Engineering (Class B) Landmark Results Incubation Fund project (BBGU-CHYLXK-KY-2022-45).

References

1. X. Rao, Ch.X. Sheng, Zh.W. Guo, Ch. Xu, L.Y. Dai and Ch.Q. Yuan, Corrosion Behaviors of Cylinder Liner in Marine Diesel Engine Burning Low Sulfur Fuel Oil: An Experimental and Molecular Dynamics Simulation Study, *Tribol. Int.*, 2022, **171**, p 107575.

2. Z.Q. Zhang, J. Ye, D.L. Tan, Z. Feng, J.B. Luo, Y. Tan and Y. Huang, The Effects of Fe_2O_3 Based DOC and SCR Catalyst on the Combustion and Emission Characteristics of a Diesel Engine Fueled with Biodiesel, *Fuel*, 2021, **290**, p 120039.
3. Z.Q. Zhang, J. Li, J. Tian, Y. Zhong, Z. Zou and R. Dong, The Effects of Mn-Basedcatalysts on the Selective Catalytic Reduction of NOx with NH3 at Low Temperature: A Review, *Fuel Process. Technol.*, 2022, **230**, p 107213.
4. X. Wang, Y. Li and J.S. Liu, Molecular Structure Design of Diesel Anti-wear Agents, *Acta Petrolei Sinica.*, 2018, **34**(2), p 229–237.
5. W. Ch Chen, J.G. Chen, H.P. Chen, N.M. Ye, B. Zhwei, L.M. Luo and Y. Ch Wu, Nanosized Copper Powders Prepared by Gel-Casting Method and Their Application in Lubricating Oil, *Trans. Nonferrous Metals Soc. China.*, 2018, **28**(6), p 1186–1191.
6. L. Zhang, Y. He and L. Zhu, Alkyl Phosphate Modified Graphene Oxide as Friction and Wear Reduction Additive in Oil, *J. Mater. Sci.*, 2019, **54**, p 4626–4636.
7. S. Kawai, A. Benassi and E. Gnecco, Superlubricity of Graphene Nanoribbons on Gold Surfaces, *Science*, 2016, **351**(6276), p 957–961.
8. B. Ricardo, S. Diego and B. Cristiano, Tribological Behaviour of Plasma-Functionalized Graphene as Low-Viscosity Oil Additive, *Tribol. Lett.*, 2018, **66**, p 114–128.
9. K. Parveen and M.F. Wani, Synthesis and Tribological Properties of Graphene: A Review, *J. Tribol.*, 2017, **13**, p 36–71.
10. A.K. Rasheed, M. Khalid and A. Javeed, Heat Transfer and Tribological Performance of Graphene Nanolubricant in an Internal Combustion Engine, *Tribol. Int.*, 2016, **103**, p 504–515.
11. P. Gayatri, S.H. Subhasis, H. Harish, K. Tapas and N.C. Murmu, Tribological Behavior of Dodecylamine Functionalized Graphene Nanosheets Dispersed Engine Oil Nanolubricants, *Tribol. Int.*, 2019, **131**, p 605–619.
12. M.N. Yang, S.L. Fan, H.Y. Huang, Y.J. Zhang, Z.Q. Huang, H.Y. Hu and J. Liang, In-situ Synthesis of Calcium Borate/Cellulose Acetate-Laurate Nano-composite as Efficient Extreme Pressure and Anti-wear Lubricant Additive, *Int. J. Biolog. Macromol.*, 2020, **156**, p 280–288.
13. R.L. Frost, Y.F. Xi, R. Scholz, F.M. Belotti and M.C. Filho, Infrared and Raman Spectroscopic Characterization of the Borate Mineral Colemanite-$CaB_3O_4(OH)_3H_2O$-Implications for the Molecular Structure, *J. Mol. Struct.*, 2013, **23**(8), p 1037.
14. Y. Li, S.W. Zhang, Q. Ding, J. Zhtang, D.F. Qin and L.T. Hu, The Extreme Pressure and Lubricating Behaviors of Potassium Borate Nano-particles as Additive in PAO, *Particul. Sci. Technol.*, 2018, **37**, p 1458353.
15. Z.F. Jia, X.J. Pang and H.Y. Li, Synthesis and Wear Behavior of Oleic Acid Capped Calcium Borate/Graphene Oxide Composites, *Tribol. Int.*, 2015, **90**, p 240–247.
16. B.H. Chen, K.C. Gu and J.H. Fang, Tribological Characteristics of Monodispersed Cerium Borate Nanospheres in Biodegradable Rapeseed Oil Lubricant, *Appl. Surf. Sci.*, 2015, **353**, p 326–332.
17. L.Y. Dai, R.G. Meng, J.F. Chen, Preparation and Application of Surface Modificated Nano Materials as Lubricating Oil additive. China. 2014, ZL 201410068071
18. G.P. Ji, X.F. He, H.F. Liao, L.Y. Dai, D. Sun and GCh. Cai, Tribological Properties of Surface Modified Cu Nanoflakes Prepared by Plasma Assisted Ball Milling, *J. Mater. Eng.*, 2019, **47**(6), p 114–120.
19. X.B. Hou, Y.J. Ma, B. Geetanj, Z.B. Yin, L.Y. Dai, H.F. Liao and Y.K. Wei, Preparation and Tribological Properties of Graphene Lubricant Additive for low Sulfur Fuel by Dielectric Barrier Discharge Plasma-Assisted Ball Milling, *Processes.*, 2021, **9**, p 272.
20. X.B. Wang, Y.F. Zhang, Zh.G. Yin, Y.J. Su, Y.P. Zhang and J. Cao, Experimental Researchon Tribological Properties of Fliquid Phase Exfoliated Graphene as an Additive in SAE 10W–30 Lubricating Oil, *Tribol. Int.*, 2019, **135**, p 29–37.
21. B.B. Wang, E.Z. Hu, Z.Q. Tu, D.K. Dearn, K.H. Hu and X.G. Hu, Characterization and Tribological Properties of Rice Husk Carbon Nano-Particles Co-doped with Sulfur and Nitrogen, *Appl. Surf. Sci.*, 2018, **462**, p 944–954.
22. V.G. Pol, L.K. Shrestha and A.K. Kumar, Tunable Functional Carbon Spheres Derived from Rapid Synthesis of Resorcinol-Formaldehyde Resins ACS, *Appl. Mater. Interf.*, 2014, **6**, p 10649–10655.
23. J. Sun, H.M. Liu, X. Chen, D.G. Evans, W.S. Yang and X. Duan, Synthesis of Graphene Nanosheets with Good Control Over the Number of Layers Within the Two-Dimensional Galleries of Layered Double Hydroxides, *Chem. Commun.*, 2012, **48**, p 8126–8128.
24. B.J. Ren, L. Gao, M.J. Li, Sh.D. Zhang, G.Q. Zu and X. Ran, Tribological Properties and Anti-Wear Mechanism of ZnO @ Graphene Core-Shell Nano-particles as Lubricant Additive, *Tribol. Int.*, 2020, **144**, p 106114.
25. L. Ouyang, L. Guo and W. Cai, Facile Synthesis of Ge@FLG Composites by DBDP Assisted Ball Milling for Lithium Ion Battery Anodes, *J. Mater. Chem. A*, 2014, **2**(29), p 11280–11288.
26. X.B. Ji and Y.X. Chen, Hydrothermal Synthesis and Tribological Properties Study of Nano-calcium, *Lubr. Eng.*, 2015, **40**(7), p 75–77.
27. D.Y. Ma, C.M. Wang and X.X. Li, Research on Preparation and Infrared Property of Graphene and Nano-copper Composites, *Acta Photonica Sinica.*, 2018, **47**(03), p 69–74.
28. L.P. Wang, H.X. Wu, D.Y. Zhang, G.N. Dong, X.H. Xu and Y.B. Xie, Synthesis of a Novel Borate Ester Containing a Phenylboronic Group and its Tribological Properties as an Additive in PAO 6 Base Oil, *Tribol. Int.*, 2018, **121**, p 21–29.
29. Zh.L. Yang, H.F. Liao, D. Sun, L.Y. Dai, Zh.J. Liu and WCh. Wang, Effect Mechanism of Plasma Assisted Ball Milling on Synthesis of Ultrafine AIN from $AI^+C_4H_4N_4$, *Chin. J. of Nonferrous Metals*, 2018, **28**(08), p 1587–1596.
30. J. Wang, XCh. Guo, Y. He, M.J. Jiang and KCh. Gu, Tribological Characteristics of Graphene as Grease Additive under Different Contact forms, *Tribol. Int.*, 2018, **127**, p 457–469.
31. K. Kavita, K.V. Jyoti, K. Dinesh, K.S. Bharat, S. Alok, S. Nivedita and B.R. Rashmi. Indrajit, Theoretical and Experimental Studies of Pyranopyrazoles and Their Tribological Compatibility with a Borate Ester, *Colloids Surf. A.*, 2020, **606**, p 125497.
32. A.V. Naumkin, A. Kraut-vass, S.W. Gaarenstroom, C.J. Powell. NIST x-ray Photoelectron Spectroscopy Database. NIST Standard Reference Database 20, Version 4.1. Assessed 14 November (2016)
33. D.K. Verma, B. Kumar and R.B. Rastogikavita, Zinc Oxide and Magnesium-Doped Zincoxide-Decorated Nano-composite of Reduced Graphene Oxide as Friction and Wear Modifiers, *ACS Appl. Mater. Interfaces*, 2019, **11**, p 2418–2430.